Virginia Journal of Science
Volume 61, Number 3
Fall 2010

Modeling and Simulation on Signatures of Mars Minerals

Widad Elmahboub[1], **Edward Yankey**, **Olivia Kerwin**,
Mathematics Department, Hampton University
Hampton VA 23668

ABSTRACT

The objective of this study was to assess the feasibility of identiying minerals on Mars using remotely sensed data. In the process we also investigated the effect of noise of aerosol and dust particles on the spectra of Mars minerals. The remotely sensed data was obtained through modeling and simulation and compared to the lab spectroscopy of the specific minerals in order to make an accurate identification. A linear model was developed using MATLAB Random Number Generator to obtain a simulated image. Part of the information we needed for the linear model was pure pixel information of Mars which was obtained from Mars Spirit images. Random noise was added to the image in order to simulate a real world image. In addition to the random noise, a mathematical model was developed to represent the noise caused by aerosols and dust particles in Mars's atmosphere. The simulation was tested to ensure that it satisfied the appropriate model testing. Our results showed that our linear model was appropriate, and was accepted at a confidence interval of about 95%. The simulated image was then corrected from noise through iterations. The overall accuracy of the corrected image showed an improvement in classification by 25%. The signatures of the spectra of the two images were obtained and compared to the lab spectroscopy of specific minerals. The degradation of noise showed improvement in the spectral analysis of Mars data. The spectral analysis showed the presence of iron oxide, calcium oxide and magnesium oxide leading to the conclusion that the image simulation is reliable in mineral spectral identification.

Key Words
Remote sensing of planetary surface, spectroscopy, and mathematical modeling

INTRODUCTION

Remote Sensing aspect of space science and technology relies mainly on sensors on satellites and mounted in telescopes to monitor Earth, other planetary bodies and distant stars and galaxies. This research is important since extraterrestrial remote sensing may make the greatest contributions to useful knowledge of value to humankind's future. Remote sensing in time became an important means of analyzing the status of what was on the planet's surface: clues as to mineral content (Avery, et.

[1]Contact information: Mathematics Department, Hampton University, 200 Eric Nelson Run, Yorktown VA 23693. E-mail: widad.elmahboub@cox.net.

al., 2001). Mars mineral identification is a growing area in scientific community. Researchers attempted to determine minerals using different approaches. However, mineral identification on Mars is underway through orbital visible-infrared remote sensing in concert with spectroscopic, chemical and magnetic measurements (J. Bishop, 2005). The objective of this research is to determine minerals in Mars in visible and the near-IR (near infrared) (0.35 – 1.4 micrometers) through modeling and simulation and remote sensing techniques as described in the Methods. The objective of this study was to identify minerals on Mars through developing a linear mixture model using remotely sensed data and compared it to the spectroscopy of the specific minerals in order to make an accurate identification . In the process we also investigated the effect of noise of aerosol and dust particles on the spectra of Mars minerals. The applications for this method are numerous, but the most significant would be to remotely determine the mineral make up of a planetary surface accurately.

METHODS

The data were extracted from the Spirit instrument MER-A (Mars Exploration Rover – A, January, 2004). In order to simulate an image composed of a mixture of minerals, end member spectra (EMS) and cover class proportions (CCP) were used.

Principle of Linear Mixture Model

In developing the simulated image, the linear mixture model approach was used. The linear mixture model includes mixtures of nine different classes for three sets of EMS representing minerals with different CCP. The requirement of the linear mixture model depends on the extraction of EMS and the CCP (Jian and Haigh 1997).

To extract the EMS from pure pixel values (X) in a homogenous part of the imagery, a certain number of training sets are predefined and each pixel is assigned to a training set that it resembles. The quality of training sets depends mostly on accuracy of the automated classifier (Lilisand and Kiefer, 1994).

If there are *c* types of ground cover and *n* spectral bands, it is always assumed that $n \geq c$ to avoid the identifiability problem. A column vector $f = [f_1, \ldots . f_c]^{\tau}$ is used to denote the proportions of areas within the pixels occupied by each of the c types of ground cover.

In correspondence with the Linear Mixture model, we can formulate the equation below:

$$x_i = \sum M_{\ddot{u}} f_i + e_i \quad , \tag{1}$$

Where $M_{\ddot{u}}$ is independent of f_i and e_i represents noise.

We can rewrite equation (1) in matrix form as:

$$X = mf + e = \mu_1 f_1 + \mu_2 f_2 + \ldots + \mu_c f_c . \tag{2}$$

to estimate $\hat{f}$ which satisfies the constraints such that:

$$\sum_{j-1}^{c} \hat{f}_j = 1, \hat{f}_j > 0, \quad \text{j = 1,…,c.} \tag{3}$$

In order to ensure that all the error is due to atmospheric noise, the least square method is used. The assumption is that the random noise is confined to E' and denoted as a column vector as E' = [E_1, …, $E2$] Then equation (2) can be modified to be (Jian and Haigh 1997):

$$X' = \hat{M}F + E' \ . \tag{4}$$

The error can be minimized by using: $\|X' - MF'\|^2$, (Jian, L., and Haigh, J. 1997). Several LS constraining methods were used to estimate the CCP which can be shown in the following.

1. Normalized Least Squares Method

If the estimated $\hat{F}_{LS}$ included a negative element of CCP, they will be set to zero, then the remaining elements will be scaled so that they all total one. For example, when *c* equals 4 classes, if a vector of the estimated CCP $\hat{F}_{LS}$ is [0.4 -0.05 0.7 -0.06], then the negative proportions -0.05 and -0.06 will first be set to zero, so as to convert to [0.4 0 0.7 0]. Secondly, each proportion will be multiplied by 1 / {sum of elements (0.4+0+0.7+0)} to yield $\hat{F}_{NLS}$ = [4/11 0 7/11 0]. Consequently, this is the closest point to $\hat{F}_{LS}$ while satisfying the constraints of Equation (3), (Settle and Drake, 1994).

2. Lagrangian Least Square Method

Settle and Drake (1994) proposed an algorithm to solve the constrained least squares problem. If the constraints of Equation (3) are satisfied, the new equation can be derived by the Lagrangian analysis, such that

$$\hat{F}_c = \alpha Uj + (1 - Uj)\hat{F}_{LS} \ , \tag{5}$$

Where j = [1,……,1] ^{T} in a $c \times 1$ matrix where the elements are all 1,

$J = jj^T$ is a c × c matrix I in a $c \times c$ identity matrix, U = (M^T M)$^{-1}$ is a $c \times c$ matrix, and α = (JUJ^T)$^{-1}$ is a constant.

Eventually, the newly constrained least squares solution ($\hat{F}_{LLS}$) can be decided such that:

$$\begin{aligned} \hat{F}_{LLS} &= \hat{F}_c && 0 \le j^T \hat{F}_c \le 1 \\ &= (I - \alpha UJ)\,\hat{F}_c && 0 \ge j^T \hat{F}_c \\ &= \alpha Uj + (I - \alpha UJ)\,\hat{F}_c && I \le j^T \hat{F}_c \end{aligned} \tag{6}$$

The solution using the Lagrangian method constraints only the sum to one condition, so the solution may include negative proportions for some elements. Therefore, after finding the solution by using Equation (6), the normalizing method that was discussed in the previous section can be applied for the negative elements.

3. Weighted Least Squares Method

A constraint can be imposed as:

$$C = \left\| \hat{M}F - X \right\|^2 + \lambda^2 \left\| 1 - jF \right\|^2 \tag{7}$$

With a very large weight factor, λ, so that, in a deviation from 1- *j*, F will cause a significant error to C. Consequently, the sum of one condition, $j'F = 1$, is effectively imposed. Equation (7) can be written as the following matrix (Settle and Drake, 1994):

$$C = \left\| \begin{bmatrix} 1 \\ \ldots\ldots 1 \\ \ldots\ldots\ldots 1 \\ \ldots\ldots\ldots\ldots\ldots \lambda^2 \end{bmatrix} \left\{ \begin{bmatrix} \hat{M} \\ 1\ldots\ldots\ldots\ldots 1 \end{bmatrix} \times \begin{bmatrix} f \\ . \\ . \\ f_c \end{bmatrix} - \begin{bmatrix} X_1 \\ . \\ . \\ X_n \\ 1 \end{bmatrix} \right\} \right\|^2 \tag{8}$$

$$C = \left\| \begin{bmatrix} .. \hat{M} \\ \lambda_1 \ldots\ldots\ldots\ldots \lambda_n \end{bmatrix} \times F - \begin{bmatrix} \lambda \\ X \end{bmatrix} \right\|^2 \tag{9}$$

Once the $\hat{M}$ and $\tilde{X}$ minimizing equation (12) are found, then:

$$\hat{F}_{WLS} = \hat{M} + \tilde{X} \tag{10}$$

Where the subscript WLS represents weighted least squares,

$$\hat{M} = \left[\frac{\hat{M}}{\lambda_1 \ldots\ldots\ldots \lambda_n} \right], \text{ and } \hat{X} = \left[\frac{X}{\lambda} \right]$$

Mathematical Atmospheric Model

The principle of the mathematical atmospheric model is that the light undergoes transformation and nonlinear change as it is scattered by aerosols while passing through the atmosphere. The set of eignvalues represents value of coefficient of the

scattering vector in space. The nonlinear change is proportional to the light intensity (Logan, 2006) as in the following:

$$I^{"} - \eta I = 0 \tag{11}$$

where η> 0.
The general solution for the intensity in equation (6) is;

$$I = A\cos \mu x + B\sin \mu x \ , \tag{12}$$

where $\eta = \mu^2$, and its derivative is,

$$I' = -A\mu \sin \mu x - B\mu^2 \cos \mu x \ , \tag{13}$$

$$I" = -A\mu^2 \cos \mu x - B\mu^2 \sin \mu x \ , \tag{14}$$

Substituting into equation (6), the following matrix is presented:

$$\begin{vmatrix} \cos \mu a - \cos \mu b & \sin \mu a - \sin \mu b \\ \sin u\mu b - \sin \mu a & \cos \mu a - \cos \mu b \end{vmatrix} = 0 \tag{15}$$

We then solve for the eigenvalues;

$$\mu_n = \frac{2n\pi}{b-a} \tag{16}$$

$$\eta_n = \left(\frac{2n\pi}{b-a}\right)^2 \tag{17}$$

The eigenvalue is assumed to be equal to the optical depth in an atmospheric layer as in the following:

$$\eta_n = \frac{K_{sca} \exp(-Z/H) * A * Z}{\cos\theta} \tag{18}$$

where K_{sca} is the scattering coefficient. Z is the altitude in kilometers, and θ, represents the zenith angle (Bohren and Huffman, 1983). This equation can be used for computation of the atmospheric noise that is intercepted by the telescope or the sensor. The atmospheric noise is represented by the following:

$$\delta = \frac{(1 + Area)K_{sca} A * B * Z * T^{pixel}}{(1 + area)K_{sca} A * B * Z + 1} \tag{19}$$

The atmospheric noise will be added to the linear mixture model equation as in the following equation:

$$X' = \hat{M} F + E' + \delta \tag{20}$$

As we mentioned previously this atmospheric noise will be degraded using iteration, trial and error iterations. The accuracy of correction can be measured by the overall accuracy of classification. The corrected image signatures will be compared to the lab spectra of minerals.

Simulation of Linear mixture model

The EMS was obtained by selecting pure pixel values from a perfectly homogenous area of Mars Spirit images, which represent different minerals. Perfectly homogenous areas are designated by similar signatures/spectral values and/or spectrally separable classes as shown by EMS data sets in Table 1. The extracted data set 1 (EMS set 1) consisted entirely of spectrally separable classes with distict signature values (threshold 10 signature values) as shown by band 3 (class1, class 2, and class 3). The EMS data set 2 (EMS set 2) is made up of a mixture of spectrally separable (band 1-class3, band 2-class 3, and band 3-class 3) and similar classes (threshold 6 signature values). The data set 3 (EMS set 3) consisted entirely of spectrally similar classes and do not show any distinct values. We obtained samples of the necessary training sets within the simulated image by using the training set signature editor in ENVI 4.4 (commercial software) where a reference cursor on the screen was used to manually delineate training area polygons in the displayed image. The pixel values within the polygons were used in the software to develop a statistical description file for each training area. The next step is estimate the CCP using the different constraining methods as described previously. Furthermore, to impose the critical constraints, which are the "sum to one" and "make all CCP positive," several methods were used, such as the Normalization, Lagrangian, and Quadratic constraining methods and the weighted constraining method (Settle and Drake, 1994). These methods were tested to determine the best constraining method for this experiment. After deciding upon CCP estimation and constraining methods, evaluations of estimating EMS and its effects on the corresponding CCP estimation were presented in the section above.

The Quadratic Programming method was tested to be the best constraining method as described in linear mixture model. Using the EMS data sets, the pixel values were computed based on Equation (2) using the MATLAB Random Number Generator. The mathematical model was used to derive the atmospheric error. The atmospheric noise errors were added to the EMS to simulate realistic data sets. As mentioned previously, a minimization of the random error in pixel value was implemented (section 2.1). An ASCII file with pixel values was produced and imported in ERDAS IMAGINE as an image file. The image is then corrected for atmospheric noise through trial and error iterations to reduce the atmospheric error and produce enhancement to the classification accuracy. The Maximum Likelihood automated classifier in ENVI (commercial software) was used. At each iteration step, the atmospheric noise was subtracted using initial values of solar zenith angles and scattering coefficient. The iterations were terminated when the overall classification accuracy reached an optimum value. The signature graphs of the corrected image are compared with lab spectra of minerals (Dalton et. al, 2005). The lab spectra of minerals are considered a "fingerprint" (Clark, 1983). If the graph behavior of corrected image signature values is matching the lab spectra of minerals, then we can conclude that the mineral is identified.

RESULTS

Three different EMS data sets or classes with nine subsets were generated in Table 1. After adding the random noise, the CCP was normalized again to make all CCP positive and equal one. The CCP was estimated using the least squares and end member spectra method (LS EMS) with different constraining methods. To avoid an unexpected random effect, we repeated the calculation several times for each noise level. The Roat Mean Square Error (RMSE) of the different combinations of CCP constraining methods by changing the noise level while using the same LS-EMS is shown in Figure 1. The different combinations of CCP constraining methods are L-LS-CCP (Lagrangian-Least Square-Cover Class Proportions), W-LS-CCP (Weighted-Least Squares-Cover Class Proportions, and Q-CCP (Quadratic programming constraining method-cover class proportions).

The different sample sizes may affect the overall results of these experiments. So, the same experiment was performed with changing the sample sizes. The RMSE of different combinations of the CCP estimation and constraining methods by changing the sample sizes while using the same LS-EMS is shown in Figure 2.

The results show that the quadratic programming method proved to be the best constraining method for CCP estimation. This is shown in Figures 1 and 2, indicating that this method performed much better because of a lower (Roat Main Square Error) RMSE, which does not change with sample size. The result was reasonable, because of adding a normally distributed error and testing the sample groups that created the data set.

The simulated image including the atmospheric effect was tested using statistical testing for appropriate model and significant regression model using SAS/STAT software. We presented some selected samples of results which show the regression is significant at 90% confidence interval. Since $F_{k-2,n-k}$ is larger than 14.25 (Milton and Arnold,1986). H_0 is accepted at $p < 0.025$ at 97.5% confidence. Therefore it can be concluded that the model is appropriate.

The simulated image for minerals with atmospheric noise/effects is shown in Figure 3. The corrected simulated image from atmospheric effects is shown in Figure 4. The correction accuracy is presented by the overall accuracies of classification at the final iteration which are shown in Tables 2, 3, 4, 5, 6, and 7. The overall accuracy of classified pixels for the image with atmospheric effect (Figure 3) is 71.42% and for the corrected simulated image (Figure 4) is 97.56%. The overall accuracy shows improvement in classification which ranges between 22% -25 %. The wavelength was plotted versus the spectral signature (spectral radiance) as in Figures 5, 6, and 7.

DISCUSSION AND CONCLUSION

Since the statistical regression test was conducted at 90 % confidence interval for the linear mixture model, we conclude that the regression model is significant. We conclude that the model is appropriate at 97.5 confidence interval. The results of classifications were presented by the error matrices for three minerals as in Tables 2, 3, 4, 5, 6, and 7. In each table, the last row includes the column total represents the truth data. The diagonal and no diagonal elements represeant the classified data The spectral values along the diagonal are higher than the off diagonal ones which indicated

higher accuracy. The overall accuracy showed improvement by 22%-25%. This indicates that the accuracy of correction is significant. We can conclude that the correction using the atmospheric model produced significant classification accuracy. Figures 5, 6, and 7 represent the wavelength versus signatures (spectral radiances) of the simulated image for three minerals that were compared with the experimental spectra of different minerals. The signatures matched the experimental lab spectra for iron oxide, magnesium oxide and calcium oxide. Thus, the spectral analysis showed the presence of iron oxide, calcium oxide and magnesium oxide leading to the conclusion that the image simulation is reliable in mineral spectral identification. The applications for this method are numerous, but the most significant would be to remotely determine the mineral make up of a planetary surface accurately.

LITERATURE CITED

Avery, T.E. and G.L. Berlin. 2001. Fundamentals of Remote Sensing and Air photo Interpretation, 6th Ed., MacMillan Publ. Co., 472 p.

Adams, J.B. 1974. Visible and Near-Infrared Diffuse Reflectance Spectra of Pyroxenes as Applied to Remote Sensing of Solid Objects in the Solar System. Journal of Geophysics Research 79:4829-4836.

Bishop, J.L. 2005. Hydrated Minerals on Mars. Pages 65-96 in Water on Mars and Life (Advances in Astrobiology and Biogeophysics) Tetsuya Tokano ed. Springer-Verlag, Berlin.

Bohren C. and D. Huffman. 1983. Absorption and Scattering of Light by Small Particles, 2nd ed., New York, NY: Wiley Interscience.

Clark, R.N. 1983. Spectral Properties of Mixtures of Montmorillonite and Dark Carbon Grains: Implications for Remote Sensing Minerals Containing Chemically and Physically Adsorbed Water. Journal of Geophys Research 88:10635-10644.

Dalton, J.B, O. Prieto-Ballesteros, J.S. Kargel, C.S. Jamieson, J. Jolivet, and R. Quin. 2005. Spectral Comparison of Heavily Hydrated Salts with Disrupted Terrains on Europa. Elsevier Inc.

Elmahboub, W. 2009. A combined methodology to produce highly accurate classification for AVIRIS hyperspectral data. Canadian Journal of Remote Sensing 35(4):321-335.

Elmaboub, W. M. 2000. An Integrated Atmospheric Correction and Classification System for Remote Sensing Data to Improve Correction and Classification .Accuracy, doctoral diss, University of Wisconsin–Madison, Madison, WI, 250 p.

Jian, L. and J.Haigh. 1997. Simulated Reflectance Technique for ATM Image Enhancement. Remote Sensing18(2):243-254.

Lilesand, T. and R. Kiefer. 1994. Remote Sensing and Image Interpretation 3rd Ed, John Wiley & Sons, New York.

Logan D.J. 2006. Applied mathematics. Second Edition. Wiley Interscience.

Milton, J.S. and J.C. Arnold. 1986. Probability and Statistics in Engineering and Computing Sciences. Mc-Graw-Hill.

Settle, J.J. and N.A. Drake. 1993. Linear Mixing and the Estimation of Ground Cover Proportions. International Journal of Remote Sensing 14(6):1159-1177.

Spiegel, M.R. and L.J. Stephens. 1999. Problems of Statistics. Third Edition. McGraw-Hill.

ACKNOWLEDGMENTS

This work was under the supervision of Dr. W. Elmahboub in the Mathematics Department at Hampton Univeristy. Mr. Yankey assisted in developing the linear mixture model using MATLAB and ENVI 4.4. Ms Kerwin assisted in writing the first draft of this paper.

TABLE 1. EMS set1, 2, and 3

EMS	Sets	Band 1	Band 2	Band 3	Label
EMS set 1	class 1	54	50	67	subset 1
	class 2	58	57	71	subset 2
	class 3	59	55	101	subset 3
EMS set 2	class 1	142	146	150	subset 4
	class 2	148	150	154	subset 5
	class 3	131	131	144	subset 6
EMS set 3	class 1	241	242	246	subset 7
	class 2	245	243	249	subset 8
	class 3	257	250	252	subset 9

TABLE 2 Corrected image of mineral 1. Higher diagonal elements than non diagonal pertain to higher accuracy being achieved with correction compared to Table 3.

Classified Data	Min. 1	Min. 2	Min. 3	Row Total
Min. 1	12	0	0	12
Min. 2	1	19	0	20
Min. 3	0	0	9	9
Column Total (truth data)	13	19	9	41

TABLE 3 Classification of the noisy image of mineral 1. Less diagonal elements and more non diganoal elements compared to Table 2 which pertain to less accuracy.

Classified Data	Min. 1	Min. 2	Min. 3	Row Total
Min. 1	**11**	8	1	20
Min. 2	2	**9**	0	11
Min. 3	0	2	**8**	10
Column Total (truth data)	13	19	10	41

TABLE 4 Classification of corrected image of mineral 2. Higher diagonal elements than non diagonal pertain to higher accuracy being achieved with correction compared to Table 5.

Classified Data	Min. 1	Min. 2	Min. 3	Row Total
Min. 1	**12**	0	0	12
Min. 2	0	**16**	0	16
Min. 3	0	0	**11**	11
Column Total (truth data)	12	16	11	39

TABLE 5 Classification of the noisy image of mineral 2. Less diagonal elements and more non diganoal elements compared to Table 4 which pertain to less accuracy.

Classified Data	Min. 1	Min. 2	Min. 3	Row Total
Min. 1	**7**	5	0	12
Min. 2	5	**11**	0	16
Min. 3	0	0	**11**	11
Column Total (truth Data)	12	16	11	39

TABLE 6 Classification of the noisy image of mineral 3. Higher diagonal elements than non diagonal pertain to higher accuracy being achieved with correction compared to Table 7.

Classified Data	Min. 1	Min. 2	Min. 3	Row Total
Min. 1	**7**	5	0	12
Min. 2	1	**13**	0	14
Min. 3	0	0	**7**	7
Column Total (truth data)	8	18	7	33

TABLE 7 Classification of corrected image of mineral 3. Less diagonal elements and more non diganoal elements compared to Table 6 which pertain to less accuracy.

Classified Data	Min. 1	Min. 2	Min. 3	Row Total
Min. 1	**8**	0	0	8
Min. 2	0	**18**	0	18
Min. 3	0	0	**7**	7
Column Total (truth data)	8	18	7	33

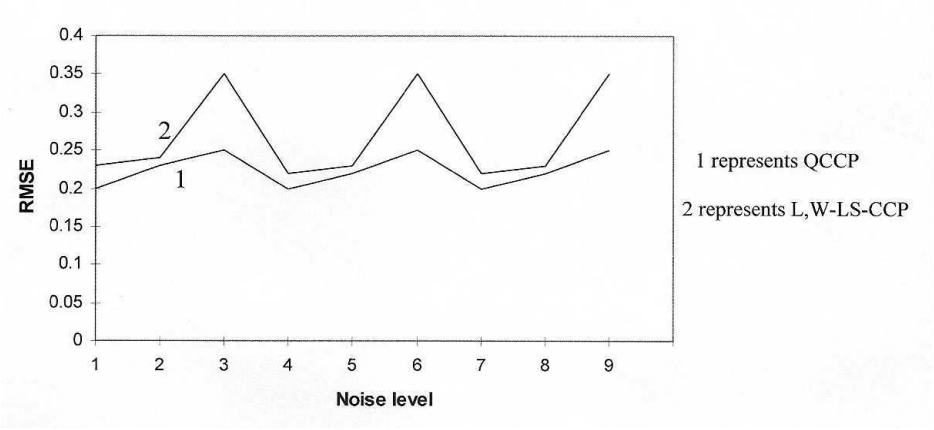

FIGURE 1. RMSE of CCP estimation and constraining methods

.

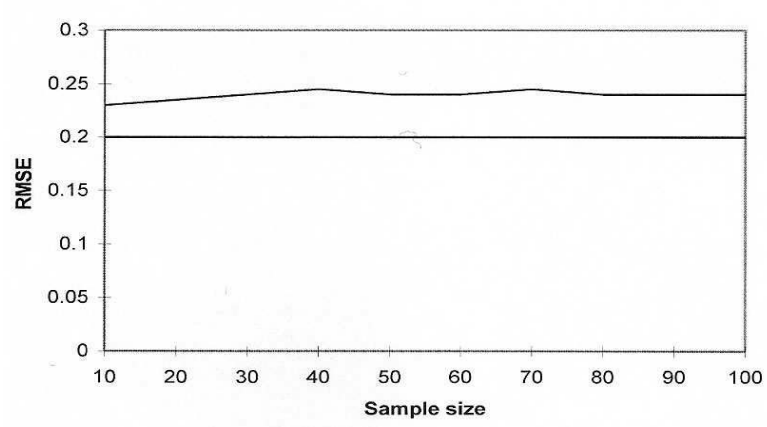

FIGURE 2. RMSE of CCP estimation and constraining methods by changing sample sizes

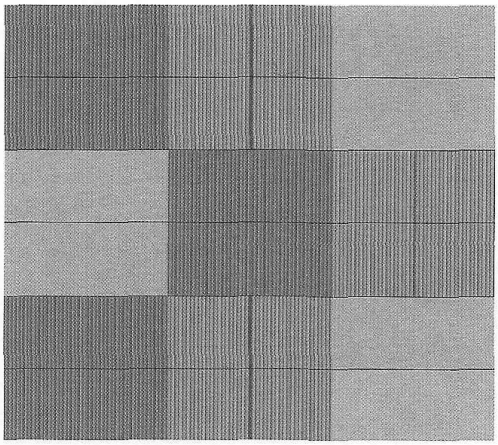

FIGURE 3. The simulated image with atmospheric noise.

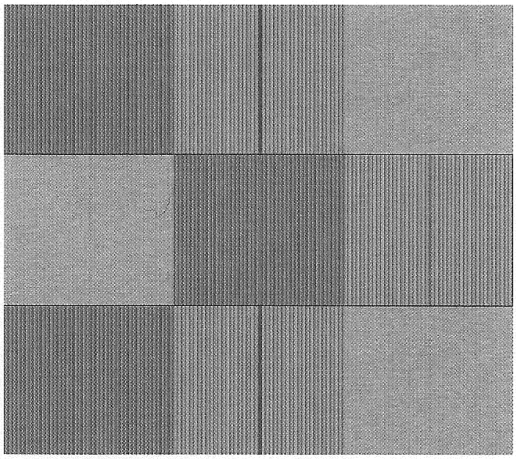

FIGURE 4. Corrected simulated image.

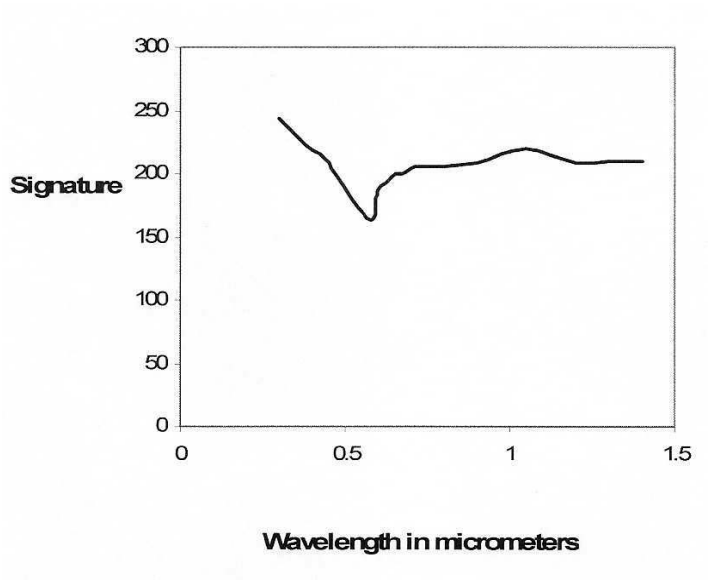

FIGURE 5. Wavelength in micrometer versus signature (in spectral radiance) shows the presence of calcium oxide when compared to lab spectra of USGS.

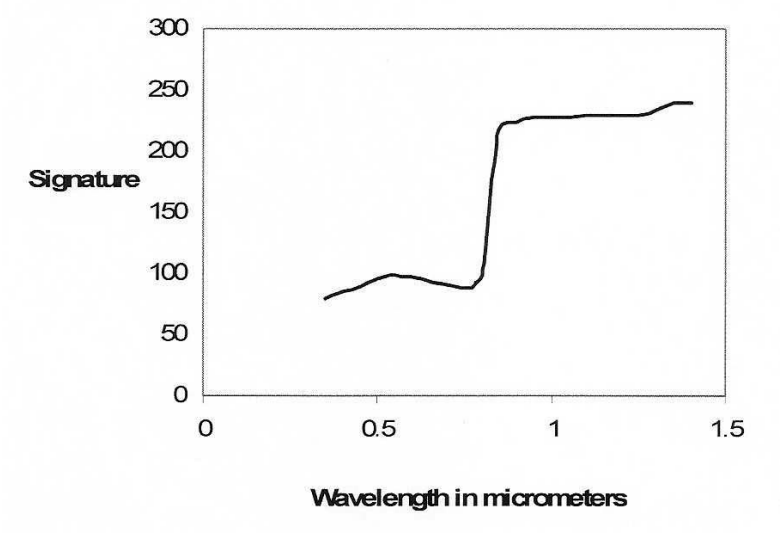

FIGURE 6 Wavelength in micrometers versus signature (in spectral radiance) shows the presence of iron oxide when compared to lab spectra of USGS.

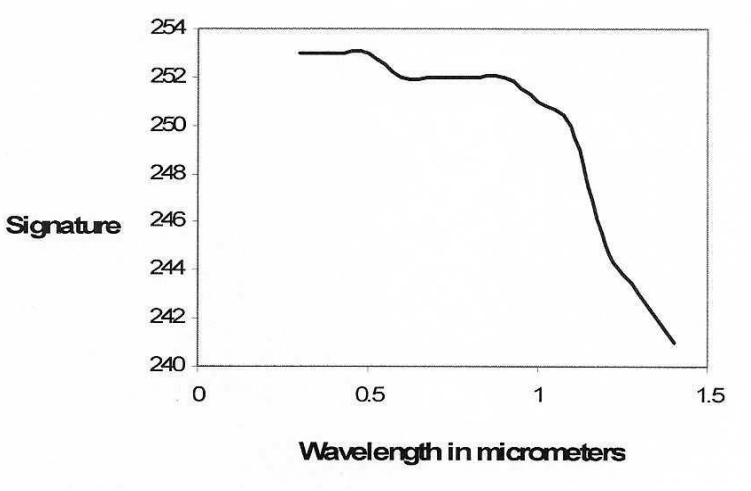

FIGURE 7. Wavelength in micrometer versus signature (in spectral radiance) shows the presence of magnesium oxide when compared to lab spectra (USGS).